Damage Progression in Thick Curved Composite Laminates under Static and Fatigue Loading

IOP Conf. Series: Journal of Physics: Conf. Series **1037** (2018) 042025 doi:10.1088/1742-6596/1037/4/042025

Damage Progression in Thick Curved Composite Laminates under Static and Fatigue Loading

B Tasdemir[3,4] and D Coker[1,2]

[1] Assoc. Prof., Dept. of Aerospace Engineering, METU, Ankara, Turkey
[2] Assoc. Prof., RÜZGEM, METU Center for Wind Energy, METU, Ankara, Turkey
[3] M.Sc., Dept. of Aerospace Engineering, METU, Ankara, Turkey
[4] Scientific Project Expert, METU Center for Wind Energy, METU, Ankara, Turkey

E-mail: coker@metu.edu.tr

Abstract. In this study, damage behavior of curved carbon fiber reinforced polymer (CFRP) composite laminates that are important sub-structures (ribs, shear webs and spar flanges etc.) for wind turbine blades are investigated under static and fatigue loading conditions. Cross-ply curved specimen consisting of groups of three 0° and 90° layers is used for clear observation of the matrix cracking in thicker plies. Damage mechanisms and locations under static and fatigue loadings are examined. In the experiments, failure is found to initiate in the first group of 90° layers under static loading while it is found to occur in the second group of 90° layers under fatigue loading. The overall goal of the project is to contribute to development of design techniques or local reinforcement methods to increase fatigue life and durability of these curved sub-structures used in wind turbine blades.

1. Introduction

In airplane wings and wind turbine blades, curved corners are commonly used in the load carrying sub-structures such as ribs, shear webs and spar flanges. Well-established damage behavior of load carrying sub-structures is the main roadmap for a safe and durable design. Increase in usage of complex composite materials due to their high strength, high stiffness with low density [1] makes it necessary to gain an understanding of the failure mechanisms of these complex composite sections. For most of wind turbine blades, glass fiber reinforced polymer (GFRP) composite material is used generally. However, wind energy industry is growing very fast and for higher efficiency, size and capacity of wind turbine blades are growing very rapidly [2]. Increase in the size of the blades brings greater deflection at the tip of the blades and heavier weight. This situation creates the necessity of using new materials [3]. To create lighter blades, carbon fibers is a good choice due to their higher stiffness than that of glass fibers. In the last decade, investigation of carbon fiber reinforced polymer (CFRP) composite material usage for wind turbine blades have increased with the performance tradeoffs [4], [5].

Wind turbine blade structures undergo cyclic loading during their entire operating life. In addition to static damage behavior, fatigue damage behavior is important for operation. In literature there are many valuable studies on static behavior of curved composite laminates [6]–[9] but there are very few studies on fatigue behavior of curved composite laminates [10], [11]. In this study, in order to clarify the damage mechanisms under static and fatigue loading, curved specimens are tested under combined moment/axial loading. Cross-ply $[0_3/90_3/0_3/90_3/0_3]_s$ specimen with grouped 0˚ and 90˚ layers are used for experimental investigations. This stacking sequence, not used in real wing designs, is chosen to isolate the effect of

matrix cracks in thicker 90˚ plies on the damage progression in multiaxial laminates. Failure is found to be initiate as matrix crack in the 90˚ plies, which then progresses to create delamination leading to loss of load carrying capacity in the beam under both static and fatigue loading. While damage initiation and growth occurs in the second group of 90˚ plies under fatigue loading, damage occurs in the first group of 90˚plies under static loading. More detailed examinations about fatigue and static behavior of curved CFRP composite laminates are presented in [12].
Main purpose of this study is to elucidate the failure mechanisms of the curved composite substructures under static and fatigue loading separately. The difference of failure location and mechanism on curved sub-structures used in wind turbine blades under static and fatigue loading may provide local reinforcement design suggestions.

2. Method

2.1. Material and Geometry

Geometry and stacking details of CFRP cross-ply 30 layer L-shaped specimen used for experimental investigations is shown in Figure 1 schematically. The arm lengths of the specimen are 90 mm and width is 25 mm with 5 mm inner radius. The CFRP composite laminates are manufactured by hand lay-up technique using HexPly® AS4/8552 UD pre-pregs. The thickness of each layer is 0.184 mm and total thickness of 30 layer the curved specimen is 5.8 mm. The excessive thickness is caused by applied excessive resin during manufacturing. The stacking sequence of the specimen is $[0_3/90_3/0_3/90_3/0_3]_s$. The layers are grouped to create thicker layers and examine the failure in detail.

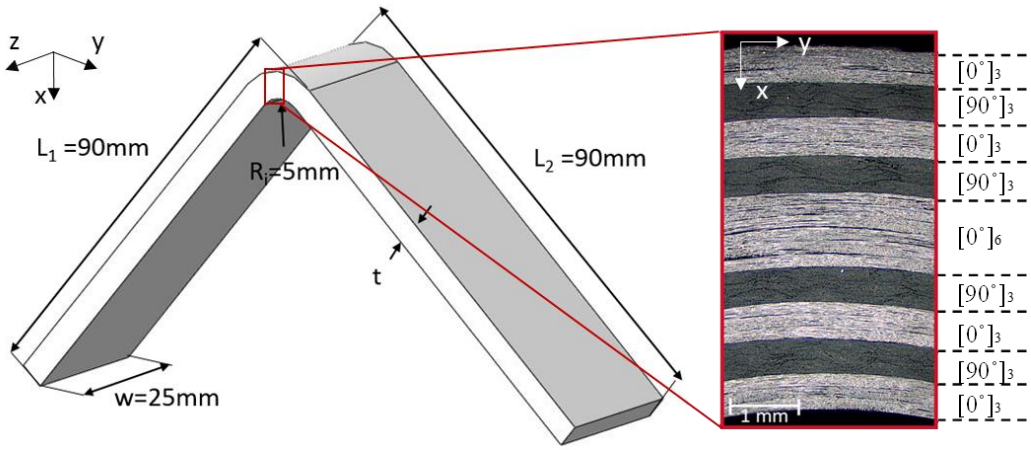

Figure 1. Geometry and stacking details of the specimen

Material properties and strength values are listed in Table 1.

Table 1. Material and laminate properties [13]

Density	ρ =1.58 g/cm^3
Elastic	E_{11}=135 GPa; E_{22}= E_{33}=9.6 GPa; ν_{12}= ν_{13}=0.32; ν_{23}=0.487; G_{12}= G_{13}=5.3 GPa; G_{23}=3.4 GPa.
Strength	F_{11}^t=2200 MPa; F_{11}^c=-1531 MPa; F_{22}^t=80.7 MPa; F_{22}^c=-199.8 MPa; F_{33}^t=80.7 MPa; F_{33}^c=-119.8 MPa; F_{12}=114 MPa; F_{13}=114 MPa; F_{23}=80 MPa

2.2. Experimental Setup

The specimen is bolted on the freely rotating pin on the loading fixture at 15 mm away from the tips of the arms and the fixture is clamped to the servo-hydraulic 250 kN static/fatigue testing machine as shown in Figure 2. Lower crosshead is moved in vertical direction and moment/axial combined loading is applied on the curved region of the specimen. In the static case, specimen is loaded at 1 mm/min under displacement control. In the case of fatigue, the specimens are loaded at 2Hz under displacement control. For specimen 1 experiment is performed between 2-4 mm displacements (R=0.5) and for specimen 2, between 1-3 mm displacements (R=0.33). For both static and fatigue experiments, the procedure is recorded by high-resolution camera images captured at 1 fps.

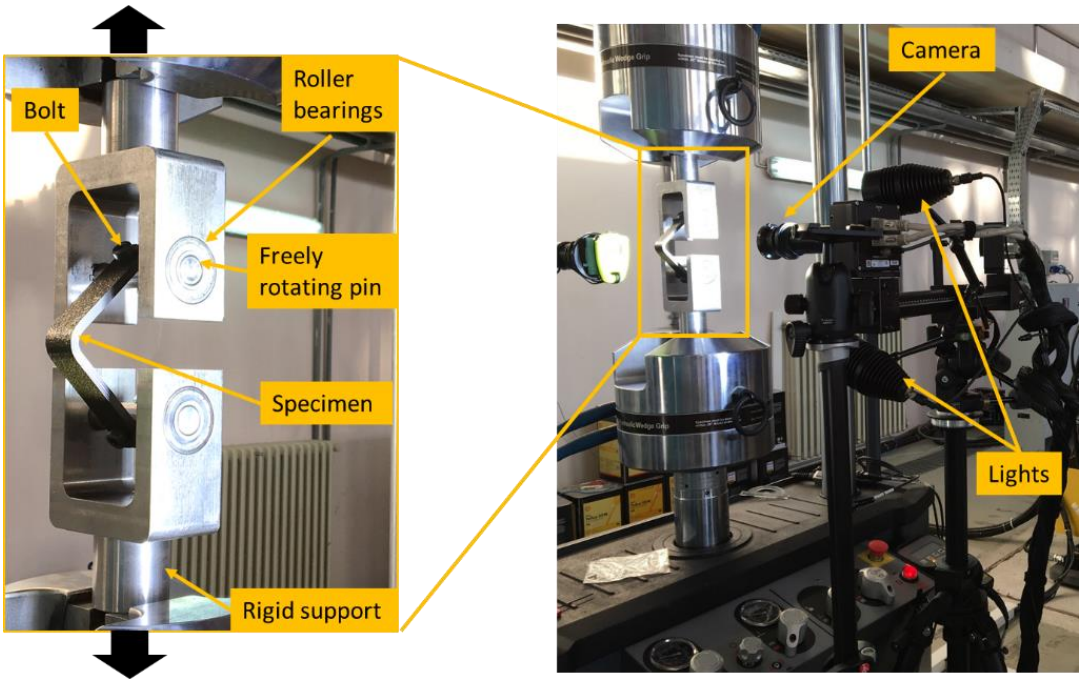

Figure 2. Loading fixture and experimental setup

3. Results

3.1. Static Results

Two 0/90 cross-ply specimens are tested under static loading. Load-displacement curves of the specimens are given in Figure 3(a). Stiffness values before and after load drop are very close to each other as seen in the load-displacement plot. In addition to stiffness values, failure loads and load reductions after failure are very similar for both specimens. Failure mechanisms of one of the specimens is given in Figure 3(b) by captured image just after the failure. The failure is observed in the first group of 90˚ layers for both specimens. It is observed that from the images, matrix crack initiate in the first group of 90˚ layers and reaches the upper 0/90 interface in the closest way and continues as a delamination.

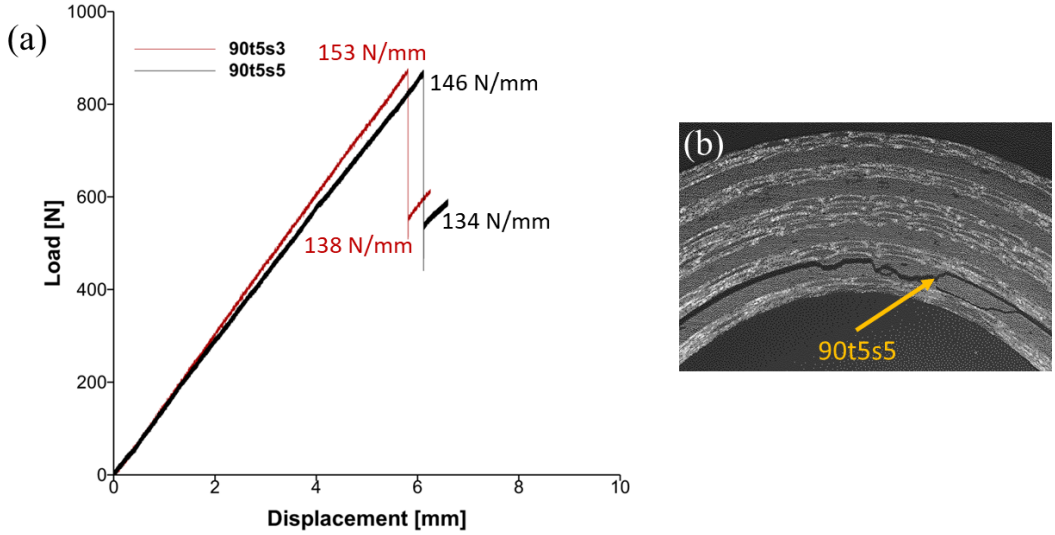

Figure 3. (a) Load-displacement plot for static experiments and (b) close-up picture of the specimen curved region after failure

3.2. Fatigue Results

One of the 0/90 cross-ply specimens, 90t5-s7, is tested under fatigue loading at 2Hz with R=0.5 while the other specimen s10 is tested at 2Hz with R=0.33. Load-displacement curves of the specimens are given in Figure 4. The specimens failed at 38000 and 58000 cycles respectively. Stiffness values before and after load drop are very close to each other as given on the load-displacement graph despite different R ratios and different failure cycles.

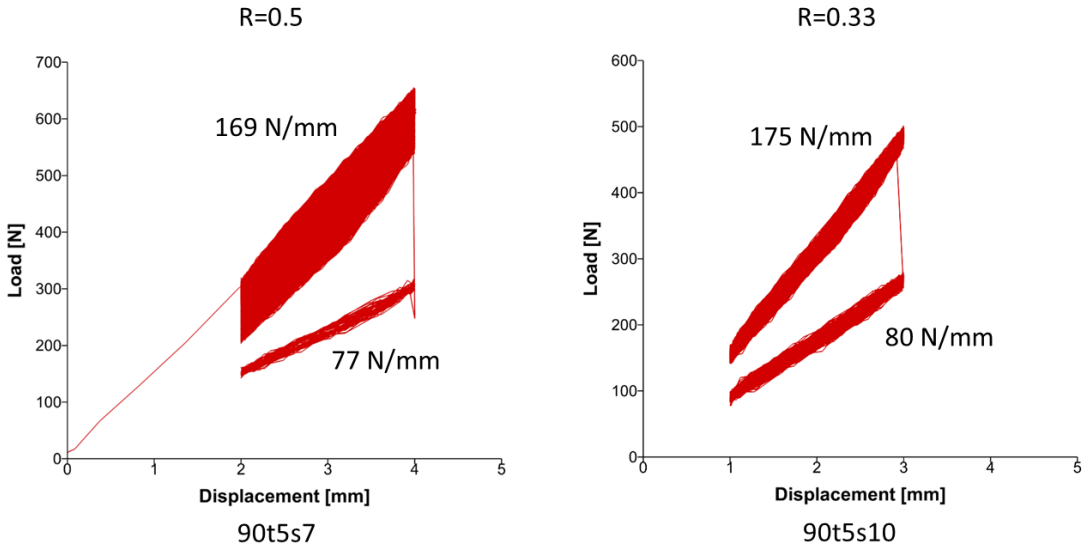

Figure 4. Load-displacement plots for fatigue experiments

Figure 5 shows a photograph of the specimen s10 after the failure. Failure in fatigue is observed to be in the second group of 90˚ layers. It is observed from the images that matrix cracks initiate in the second group of 90˚ layers and reaches the upper 0/90 interface at a shallow angle, taking a circuitous path in the 90 plies. This pattern and location is consistent in both experiments.

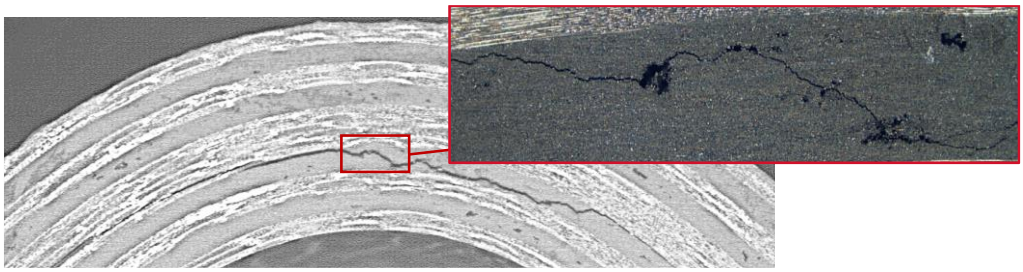

Figure 5. Location of failure on the post-failure image under fatigue loading and defect sensitivity of fatigue loading by a micrograph

Detailed micrograph examinations show that crack initiates and propagates in the second group of 90˚ layers following the visible manufacturing defects and reaches the upper 0/90 interface and continues as an interlaminar delamination as seen in Figure 5. By following the defects, the crack takes meandering path in the group of 90˚ layers up to 0/90 interface in the fatigue experiments. However, cracks under static loading attempt to reach the 0/90 interface by the shortest possible path without following the defects. This is caused by cyclic loading which leads to enlargement of the manufacturing defects and the large defects on the path joining the propagating main crack. Manufacturing defects are visible also in the first group of 90˚ layers as in second group. However, fatigue failure chooses the second group of 90° plies.

4. Discussion

Experimental results show that, for the static case, failure is observed in the first group of the 90˚ layers. On the other hand, for fatigue case failure is observed at the second group of the 90˚ layers. To investigate the reason, stress distributions on the layers are calculated by multilayer stress solution of curved composite laminates [14], [15]. Radial and tangential stress distributions at the center of the curve through the thickness are given in Figure 6. As seen from the stress distribution graphs, radial stress is maximum at second group of 90˚ layers. Radial stress is the most effective stress on the opening of existent defects. Existent manufacturing defects are enlarged in the maximum radial (opening) stress location which is the second group of 90˚ layers under cyclic loading and enlarged cracks weaken the region by decreasing the residual strength of the layer with number of cycles. As a result, when the residual strength decreases below the maximum radial stress in the material (which is in the 2nd group of 90˚ layers), macroscopic fatigue matrix cracks grow and lead to delamination.

For the case of static loading, failure occurs suddenly and does not follow the manufacturing defects, since, there is no time for the existing defects to grow and weaken the region. Due to combined stresses, failure occurs in the inner part of the curved region (first group of 90˚ layers).

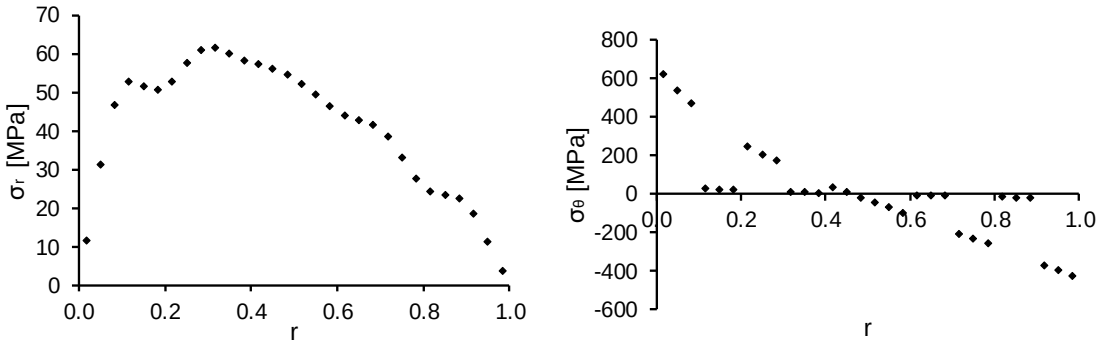

Figure 6. Radial and tangential stress distributions at center of the curve through the normalized thickness

The stiffnesses are shown in Figure 7 for static and fatigue cases. The initial stiffness for fatigue loading is found to be 10% different due to the loading rate being different. The stiffness degradation in fatigue only occurs in the last cycle with failure. In addition to failure mechanisms, percentage decrease in stiffness is different for static and fatigue cases. The graph of the stiffness degradation in Figure 7 shows that, in the fatigue experiments stiffness degradation occurs in almost the same amount for the two different R ratios and different failure cycles. For static experiments, the stiffness reduction is lower than the fatigue case. This is caused by the different failure locations. Static failure divides the curved region into two parts from the inner part of the curve leaving a thicker piece of the laminate which has a higher bending stiffness than the thinner piece that is left intact after fatigue failure.

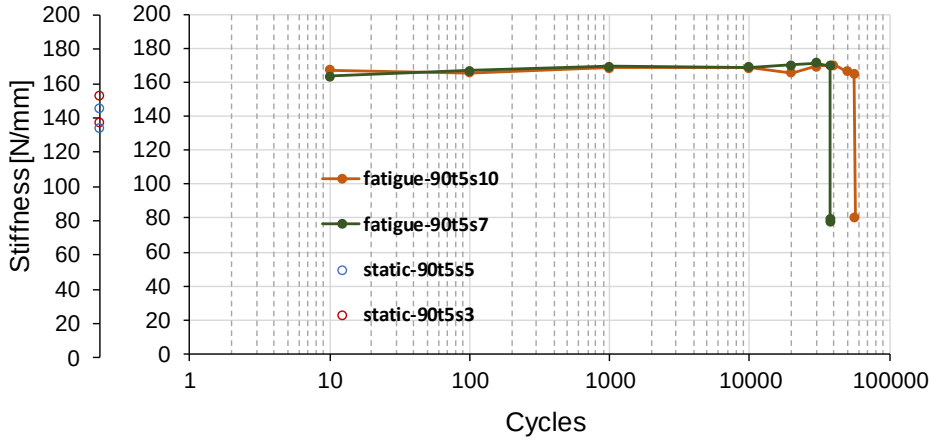

Figure 7. Stiffness degradation graph for both fatigue and static experiments

5. Conclusions

In this study, curved beam experiments under combined moment/axial loading show that failure mechanisms for static loading are different than that for fatigue loading. For both static and fatigue observations for $[0_n/90_n]$ laminates, damage initiation occurs by matrix cracking in the 90˚ plies followed by delamination at the interface of 0° and 90° plies. However, the location of the failure and the failure pattern of the matrix cracking are found to be different between the two cases [12], [16]. For static loading, it is observed that failure starts at the first group of 90˚ layer due to combined stress failure criteria and the matrix crack reaches the upper 0/90 interface in a shortest way directly by roughly 45˚ angle. For fatigue loading, it is observed that failure starts at second group of 90˚ layer at maximum radial stress location and the matrix crack reaches the upper 0/90 interface in a circuitous path smoothly by uniting the enlarged manufacturing defects under cyclic loading due to opening stresses. Additionally, residual stiffness under fatigue loading is 45% of original stiffness whereas in static loading the final stiffness is 90% of the original stiffness.

Clear understanding of the failure location, mechanism and stiffness degradation on curved sub-structures used in wind turbine blades under static and fatigue loading can provide suggestions for new locally reinforced designs for higher operating lifetime.

Acknowledgements

The authors would like to acknowledge to RUZGEM -METU Center for Wind Energy. The authors also would like to thank Tamer Tahir Ata and Ahmet Çevik for their support and assistance during the experiments and analyses.

References

[1] P. T. Curtis, “The fatigue behaviour of fibrous composite materials,” *J. Strain Anal. Eng. Des.*, vol. 24, no. 4, pp. 235–244, 1989.

[2] C. W. Kensche, "Fatigue of composites for wind turbines," *Int. J. Fatigue*, vol. 28, no. 10 SPEC. ISS., pp. 1363–1374, 2006.
[3] R. P. L. Nijssen, *Fatigue Life Prediction and Strength Degradation of Wind Turbine Rotor Blade Composites*. KC-WMC, 2006.
[4] P. S. Veers *et al.*, "Trends in the design, manufacture and evaluation of wind turbine blades," *Wind Energy*, vol. 6, pp. 245–259, 2003.
[5] D. A. Griffin, "Blade System Design Studies Volume II : Preliminary Blade Designs and Recommended Test Matrix," *SAND2004-0073*, vol. II, no. June, pp. 3–75, 2004.
[6] R. H. Martin, "Delamination failure in a unidirectional curved composite laminate," *Compos. Mater. Test. Des. astm stp 1120*, vol. 10, pp. 365–383, 1992.
[7] G. Wimmer, C. Schuecker, and H. E. Pettermann, "Numerical simulation of delamination in laminated composite components - A combination of a strength criterion and fracture mechanics," *Compos. Part B Eng.*, vol. 40, no. 2, pp. 158–165, 2009.
[8] S. Feih and H. S. Shercliffa, "Composite failure prediction of single-L joint structures under bending," *Optoelectron. Lett.*, vol. 8, no. 2, pp. 121–124, 2012.
[9] B. Gozluklu, I. Uyar, and D. Coker, "Intersonic delamination in curved thick composite laminates under quasi-static loading," *Mech. Mater.*, vol. 80, no. PB, pp. 163–182, 2015.
[10] R. H. Martin and W. C. Jackson, "Damage prediction in cross-plied curved composite laminates," *ASTM Spec. Tech. Publ.*, no. 1156, pp. 105–126, 1993.
[11] J. P. Blanchfield and G. Allegri, "F," *19th Int. Conf. Compos. Mater.*, pp. 1–9, 2013.
[12] B. Tasdemir, "Fatigue and Static Behavior of Curved Composite Laminates," Middle East Technical University, 2018.
[13] C. S. Lopes, P. P. Camanho, Z. Gürdal, P. Maimí, and E. V. González, "Low-velocity impact damage on dispersed stacking sequence laminates. Part II: Numerical simulations," *Compos. Sci. Technol.*, vol. 69, no. 7–8, pp. 937–947, 2009.
[14] S. G. Lekhnitskii, "Anisotropic Plates," *Anisotropic Plates*, p. 477, 1969.
[15] W. Ko and R. Jackson, "Multilayer theory for delamination analysis of a composite curved bar subjected to end forces and end moments," *Nasa, Tm-4139*. 1989.
[16] B. Tasdemir and D. Coker, "Damage Progression in Curved Composite Laminates under Combined Moment/Axial Fatigue Loading," in *ICCS20 20th International Conference on Composite Structures*, 2017.